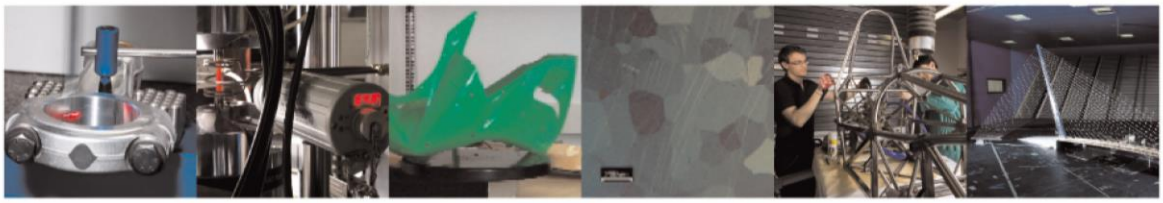

Dynamic behaviour of miniature laser textured skis

Ripamonti, Francesco; Furlan, Valentina; Savio, Alessandro; Demir, Ali Gökhan; Cheli, Federico; Ossi, Paolo; Previtali, Barbara

This is an Accepted Manuscript of an article published by Taylor & Francis in SURFACE ENGINEERING on 03 Sep 2018, available online:
https://doi.org/10.1080/02670844.2018.1512730

DIPARTIMENTO DI MECCANICA ■ POLITECNICO DI MILANO
via G. La Masa, 1 ■ 20156 Milano ■ EMAIL (PEC): pecmecc@cert.polimi.it
http://www.mecc.polimi.it
Rev. 0

Dynamic behaviour of miniature laser textured skis

Francesco Ripamonti [a], Valentina Furlan [a], Alessandro Savio[b], Ali Gökhan Demir [a], Federico Cheli[a], Paolo Ossi[c] and Barbara Previtali
[a]Department of Mechanical Engineering, Politecnico di Milano, Milan, Italy
[b]Department of Aerospace Engineering, Politecnico di Milano, Milan, Italy; [c]Department of Energy, Politecnico di Milano, Milan, Italy

ABSTRACT
Friction between moving bodies in mutual contact is a field studied in depth. A strategy to improve the tribological performance of mechanical components consists of modifying the surface microstructure using the laser surface texturing (LST) technique. For instance, the technique was shown to improve tool life and reduce energy consumption in applications concerning industrial manufacturing and automotive industry. Concerning sports equipment, e.g. skis, these are tribological systems different from generic mechanical components, and as such they require further attention to exploit the benefits of textured surfaces. In this work, LST was applied in the form of microholes (dimples) on two metallic materials, namely AISI 301 and a commercial aluminium alloy (Titanal®), used for ski manufacturing. Geometrical-morphological characteristics of the textured surface and their wettability were investigated. Finally, prototype mini-skis were manufactured and tested under different ambient snow and speed conditions. Results show that LST can reduce the friction coefficient and improve performances.

Introduction

When the dynamic contact of a body with ice or snow is studied, the development of a surface with good sliding properties represents an important issue. The ice friction mechanism is still a controversial (debated) topic in a wide range of applications. Indeed, low friction materials are welcome in the design of structures whose functions may be seriously affected by ice, e.g. aeroplanes, offshores in glacial regions and icebreaker ships [1-6]. Moreover, minimising friction against ice/snow is crucial in com-petitive winter sports like ice skating, bobsledding, cross-country skiing and alpine skiing [7-11].
Scientific investigations of ice/snow friction began around the mid-nineteenth century. M. Faraday studied the contact between two ice cubes. His conclusions were clear: ice surface is covered by a liquid-like layer [12], entirely governing the friction mechanism. This result was the starting point for further researches. About 80 years later, Bowden and Hughes suggested that frictional heating, leading to ice melting, was the main contri-bution to ice friction problems [7]. This approach is nowadays the generally accepted theory to explain fric-tion not only on ice but also on snow. This is not sur-prising once we keep into account that snow, after being deposited, is a highly porous, sintered material made of continuous ice skeleton and a continuously connected pore space, that kept together constitute the snow microstructure [13]. The time elapsing snow meta-morphism leads to material densification, formation of firn and later to ice. Not surprisingly, the exhaustive review on snow friction provided by Colbeck [8], shows that many similarities exist between snow and ice friction [14]. Experiments on ice are preferred because, given its structural and mechanical stability, its behaviour is less complex [7,9,15-18]. The sliding friction on ice is determined by many factors, such as temperature [9-11,15,19-25], sliding velocity [20,26-31], normal force [15,20,30], apparent contact area [7,17,21], roughness [24,32-34], surface wettability [16,34,35], surface morphology that is commonly known as ‘texture’ [24,34], relative humidity [27] and thermal conductivity [24,28]. All these factors affect the thickness and continuity of the liquid-like layer at the interface between the sliding body and the cold ice surface. This layer is generated by the heating associated with friction that melts part of the ice on the surface [9,14]. However, it is not always easy, nor is it con-venient, to investigate the effect of a single parameter without considering its interdependence with other fac-tors. For instance, in this context, the effect of wettability is often investigated in combination with other material parameters, such as roughness, texture and thermal conductivity [16,34,35]. Concerning this, many studies [36-43] show that friction on ice is lower for surfaces presenting a hydrophobic behaviour. Benefits are expected, especially close to the ice melting point [9,16,18,34,35], but also at lower temperatures where the melted liquid-like layer is lacking [9].

Moving from this point, it is noteworthy that surface hydrophobicity can be induced by a suitable design of surface texture. Particularly, fractal structures [44], dual-scale hierarchical structures [35,45], random hierarchical structures [46], textures with posts [47] and textures with dimples [38-42,44,47] have been investigated. In particular, random hierarchical structure pat-terns and dimple textures also allow higher wear tolerance and damage (scratch) tolerance. These tex-tures can be obtained by means of different techniques. For polymers, moulding can be adopted [47], while etching can be used with silicon specimens [45]. Otherwise, Laser Surface Texturing (LST) is suitable for metals, polymeric and ceramics materials [41,48-54]. Kietzig et al. created a dual scale roughness, using a femtosecond fibre laser, in order to change surface wettability, obtaining super-hydrophobic metallic sur-faces [35]. Demir et al. realised random surface textures and dimples employing a nanosecond fibre laser, in order to change surface wettability [55,56] and pro-mote a polymeric coating adhesion [57]. In tribological applications, LST is used to achieve wear reduction and enhanced lubrication, especially in automotive and aerospace fields [41,42]. Yet there is a lack of friction estimation of a LST sample on a snow surface, and there are only few studies on ice friction [14,34,35].

In this work, the use of LST on advanced winter sport equipment subject to snow friction is investi-gated. Two different metals, a stainless steel and a com-mercial aluminium alloy, were tested. An industrial nanosecond fibre laser was used to texture the metal surfaces with micrometric dimples. Dimple geometry was studied as a function of laser parameters. The effect of the different surface textures along with the material type on surface wettability was investigated. Prototype mini-skis with textured and plain bases were tested under different ambient conditions to evaluate the snow friction coefficient.

Materials and methods

Two metallic materials were investigated as novel alternatives to ski manufacturing. Cold rolled AISI 301 grade austenitic stainless steel was selected for its high strength and corrosion resistance. A commercial aluminium alloy, namely, Titanal® (AMAG rolling GmbH, Ranshofen, Austria), which is currently used in ski production due to its good torsional stiffness and vibration damping, was also tested. Both the materials were 0.5 mm in thickness. Mechanical prop-erties and nominal compositions of the two materials are reported in Tables 1–3.

Laser surface texturing

An industrial nanosecond pulsed fibre laser source (IPG Photonics YLP 1/100/50/50) was employed for surface texturing. Sample surface rastering was per-formed using a scanner head (TSH 8310 by Sunny Technology, Beijing, China) equipped with f-theta lens having 100 mm focal length. In this optical configuration, it is possible to obtain a minimum beam spot diameter (d_0) of 39 μm. The characteristics of the system we used are summarised in Table 4. Before laser texturing, samples were mechanically cut, then washed in ultrasonic bath with acetone for 10 min. Laser texturing was realised in order to obtain controlled dimple patterns. A point-by-point laser per-cussion drilling strategy was adopted to texture the sur-faces. The strategy consisted in sending a train of laser pulses on a defined position and jumping to the next one with a defined pitch (p), as shown in Figure 1. While the dimple pitch (p) is controlled by the scanner, the diameter and depth are controlled by the laser pro-cess parameters. The modulation duration (t_{mod}) was identified as the main control parameter [58]. We pre-liminary investigated the effect of modulation time (t_{mod}) on dimple geometry. Both materials were pro-cessed with modulation duration ranging between 30 and 80 μs. Focal point was fixed at the material surface and the pulse repetition rate was fixed at 50 kHz. Square patches of 10×10 mm^2 were realised for each condition with a fixed pitch of 100 μm along both hori-zontal and vertical directions. All textured conditions were realised in air without gas assistance. Laser textur-ing parameters are listed in Table 5.

Surface qualification

Images of the dimples were taken to investigate the sur-face morphology of each metal through a Scanning Electronic Microscope (GEMINI Column from Carl Zeiss SMT, Oberkochen, Germany). Dimple diameter and depth were measured using an optical profilometer (InfiniteFocus from Alicona Imaging GmbH, Graz, Austria). For each condition, five dimples were ran-domly selected and measured. Average values and relative standard deviations were calculated for each tested condition. A static contact angle (CA) measurement was performed on the textured patches, using the ses-sile drop method with pure water [59]. Two processing

conditions representative of different textures were chosen for further analysis. These conditions were studied after manual removal of burr by using 1200 mesh abrasive paper. For both metals, surfaces were grinded until the complete removal of the burrs, with-out modifying the original dimple diameter. Contact angle measurements were performed before and after burr removal. Candidate surface textures were chosen for each material in terms of the contact angle value, where higher contact angles were sought. All the CA measurements were performed one week after the laser texturing to be sure that the sample surface reached a steady condition [60,61].

Dynamic tests

Finally, dynamic tests were performed to investigate LST effect on snow friction. Tests were performed on scaled prototype miniaturised skis. The prototype skis consisted of a 200 × 20 mm aluminium sample holder (5 mm thickness) with a curved tip, to which the thin textured plate under investigation was rigidly connected (see Figure 2). The aluminium support provides stiffness and weight to the prototype ski. Moreover, a static load is applied on each prototype ski in order to achieve a uniform pressure distribution of 2.75 kPa, reproducing the standard operating condition experienced by a full-scale ski moving straight on a slope on the fall line. For each material, three prototype skis were prepared with the following conditions:

. one ski was provided with the non-textured base material surface (reference case)
. one ski with the selected laser textured surface
. one ski with the selected laser textured surface after burr removal.

All the tests were performed on natural snow track. Experiments were carried out in the north of Italy (Piani di Bobbio, LC) at an altitude of about 1600 m.

In order to describe the system dynamics, the model of a body sliding down along an inclined plane under the gravity effect was adopted (Figure 3(a)). According to the model, the friction coefficient μ can be expressed as:

$$m(t) = \tan(a) - \frac{a(t)}{g\cos(a)} \qquad (1)$$

where α (deg) is the track slope, g (m s^{-2}) is gravity acceleration and a(t) is body acceleration [m s^{-2}].

Prototype skis were tested on a linear track inside a

15–25 mm-deep channel. A measuring tape was unrolled parallel to the channel, in order to show the position of the prototype skis along the track. More-over, coloured sticks were positioned every 100 mm along the track. For each ski prototype, three runs on the track were performed. On each run, the prototype was released, moving from the top position with null initial velocity, sliding down freely. Each run was filmed from a lateral view by a 100 fps camera (GoPro Hero 3 Black Edition from Woodman Labs, San Mateo, USA). The video allowed us to record experimental points in terms of position (s) of the ski as a function of time (t).

Starting from a preliminary evaluation of the col-lected data, a parametric function of acceleration (a) vs time (t) is proposed

$$a(t) = \frac{1}{At2 + Bt + C} \qquad (2)$$

so that the resulting model of friction has to be consist-ent with the results provided by literature [14,18,23,62]. In particular, the function shape and the value of par-ameters A, B and C is chosen to:

. abide by the maximum acceleration limit

($m = 0$, $a = g \sin \alpha$)
. reach an asymptotic speed (v) value ($t1$, $a \to 0$, $v \to v_{lim}$) for the a(t)
. allow no more than one maximum in t [[0, 1) for the a(t).

Then, a double integration of a = a(t) allowed to get the distance function s = s(t), with the initial conditionsv(0) = 0, s(0) = 0. A Least Square Method best fit to the experimental data with s(t), returned the optimal parameters A, B and C. Finally, $m = m(t)$ was computed through equation (1), the results being displayed in terms of m versus v, both being known at each time value.

Environmental conditions play a significant role in the results of the tests [14]. For this reason, measurements of temperature and relative humidity were taken before and after each run, in order to conduct the test in constant ambient conditions. Air temperature was measured by means of a standard liquid-in-glass thermometer. Snow temperature and relative humidity were measured putting into the snow a temperature – humidity detector (107240 by Avidsen, Chambray-Iès-Tours, France). In Table 6, the conditions for each day of test are reported.

Results and discussion

In this section, the main results in terms of surface morphology assessment, wettability and dynamic performance of prototype miniaturised skis are reported.

Analysis of dimple quality and geometry

The analysis on dimple morphology showed different interaction between the materials and the laser beam. Qualitative analysis of SEM images shows a marked influence of t_{mod} on dimple structure, which is directly affected by the laser – material interaction. In Figure 4, SEM images show the effect of three modulation time values on AISI 301 and Titanal®. In both materials, an increase in burr formation with increasing t_{mod} is observed. In dimples realised on Titanal® substrate, burr formation and melted materials seem to affect a larger portion of the area adjacent to each dimple (Figure 3(e,f)) that appears rougher in comparison to dimples produced on AISI 301 (Figure 3(b,c)).

Dimple diameters and depths, measured by optical profilometer, are reported in Figures 5 and 6. For both materials, different values of t_{mod} lead to different laser ablation mechanisms known as gentle ablation and strong ablation [63]. Particularly, an increase in t_{mod} generates an increase in dimple diameter and depth. Figures 5 and 6 allow for a quantitative compari-son between dimpling of AISI 301 and dimpling of Titanal®. The process could realise dimple diameters between 20 and 35 μm on AISI 301 and between 5 and 55 μm on Titanal. Similarly, dimple depth varied over a much larger range for Titanal®, ranging between 1 and 50 μm as opposed to a range between 5 and 30 μm for AISI 301. In terms of a basic comparison, the machining rate of Titanal® appears to be higher than AISI 301.

Wettability evaluation

Sessile drop tests indicate that LST induces a significant change in surfaces wetting properties compared to the original surface. Results for textured samples in AISI 301 are reported in Figure 7. The data show that the original surface is hydrophilic with a contact angle of 74°. Contact angle values change as a function of laser process parameters, being in particular sensitive to the dimple depth trend. Laser surface texturing applied with t_{mod} greater than 50 μs produces hydrophobic surfaces (contact angle values higher than 90°). Higher values of t_{mod} leads us to an increase of the contact angle up to 128°. For values of t_{mod} between 55 and 70 μs, the variability range is wider than 20° but the surfaces always show hydrophobic behaviour.
Contact angle measurements for samples in Tita-nal® are reported in Figure 8. The untextured Titanal® showed a hydrophilic behaviour with a contact angle of 77 ± 10°. In this case, all texturing conditions produced hydrophobic surfaces with contact angles higher than 90°. In particular, t_{mod} lower than 50 μs correspond to average contact angles between 103° and 109°, whereas for higher values of t_{mod}, values up to 130° were observed. For all Titanal® samples, the variability range remained bounded within 11°.

The influence of the burr on surface wetting properties was evaluated on patches obtained with t_{mod} equal to 50 μs and 70 μs corresponding to shallow and deep dimple conditions respectively. Table 7 collect contact

angle values before and after burr removal. We notice that the mechanical polishing process does not induce any significant change of the wettability behaviour.

Dynamic analysis of friction coefficient

Dynamic analysis, in terms of sliding performance, is reported in terms of friction coefficient versus speed plots, for two test conditions:

. Test 1: 'Hot Day' conditions (air temperature= +10°C, snow temperature=+2°C, RH = 82%)
. Test 2: 'Cold Day' conditions (air temperature= −1°C, snow temperature=–1°C, RH = 73%)

Results of Test 1 are reported in Figure 9 (AISI 301) and Figure 10 (Titanal®), respectively. The base surfaces are used as reference conditions and defined as 'untextured'. Laser textured surfaces are referred to as 'LST'. Surfaces treated with laser texturing and sanding of the burrs are referred to as 'LST grinded'. In all the tests, a constant limiting speed was achieved, implying a null acceleration. Based on Equation (1), if the body moves at constant speed, the asymptotic fric-tion coefficient ($m = m_{lim}$) depends exclusively on the track slope. Concerning the AISI 301 samples (Figure 9), the LST grinded ski showed the best sliding prop-erties for the observed range of speeds. On the other hand, the performance of the LST and untextured skis was poor. For Titanal® (Figure 10), the LST grinded skis showed better sliding properties only in the initial stage of each run. With the speed increased, the coefficient of friction of the LST grinded ski became larger than the coefficient of friction of the untextured ski. The LST ski showed the poorest slid-ing properties.
Results of Test 2 are reported in Figure 11 (AISI and Figure 12 (Titanal®), where the same termi-nology as for the Test 1 is adopted. In these ambient conditions, different speeds lead to different results. For AISI 301 (Figure 11), the best performances in the initial stage of each run were obtained by the untex-tured ski, while, for higher speeds, the friction curve of the LST grinded ski lies beneath the curve of the untex-tured ski. Regardless of speed, the LST ski showed the poorest sliding properties. For Titanal® (Figure 12), the best performances in the initial stage of each run were obtained by the LST grinded ski, while, for higher speeds, the friction curve of the LST grinded ski lies above the curve of the untextured ski. Also for Titanal®, regardless of speed, the LST ski showed the poorest sliding properties.
Overall, the results show improved sliding per-formance of the textured and polished AISI 301 sur-faces. The results underline that the material, texture and finishing operation have to be considered together in order to optimise the performance of the skis. It can be deduced that the LST on its own can be detrimental to the ski sliding performance, unless the burrs are removed. The burrs can generate an interlocking mechanism [64] with the snow, which is not easily captured by the sessile drop test. The benefit of the increased water contact angle is exploited, when the surface is free from protrusions and undercuts. The choice of AISI 301 appears to be more effective compared to Titanal. The influence of material is more complex to be resolved, since the applied dimple patterns were similar in geometry with comparable levels of wettability. The local ther-mal phenomenon, which has not been strictly studied within this work, could have played a role in changing the friction behaviour. Al alloys are known to conduct heat better compared to stainless steels. In the absence of effective heat conduction, temperature increase can be expected to be higher for AISI 301 samples. The formation of a local liquid barrier between the ski and snow could have enhanced the sliding behaviour. Further investigations are required to verify such phenomenon.

Perspective

In the present work, innovative metallic bases for winter sport equipment with improved sliding performances on snow have been investigated. Two different metallic materials, AISI301 and Titanal®, were laser-textured with a dimple geometry. Beam material interaction revealed two different trends with a stronger effect on Titanal® substrate, resulting in dee-per dimples and the surrounding surface covered by melted material. Different laser parameters were tested for both materials in order to control pattern properties and to change surface wettability that directly correlate to sliding performance. LST substrate, in both cases, affects wettability that changes from hydrophilic behaviour of base material to hydrophobic. Two con-ditions were selected as ideal for each material, based on dimple patterning and wettability. The effect of burr removal on surface wettability was analysed revealing no change in contact angle values for both AISI301 and Titanal®.

Finally, selected conditions were tested in order to estimate the snow-ski friction coefficient for differently prepared miniaturised skis, considering the base material as reference case. Unlike results obtained in wettability investigation, burrs affect snow friction behaviour. Particularly, for both materials performance increases and friction coefficient reduces for LST sub-strate post processed via mechanical polishing with burr removal.

References

[1] Andersson LO, Golander CG, Persson S. Ice adhesion to rubber materials. J Adhes Sci Technol. 1994;8:117– 132.

[2] Frankenstein S, Tuthill AM. Ice adhesion to locks and dams: past work; future directions? J Cold Reg Eng. 2002;16:83–96.

[3] Laforte JL, Allaire MA, Laflamme J. State-of-the-art on power line de-icing. Atmos Res. 1998;46:143–158.

[4] Croutch VK, Hartley RA. Adhesion of ice to coatings and the performance of ice release coatings. J Coat Technol. 1992;64:41–52.

[5] Golovin K, Kobaku SPR, Lee DH, et al. Designing dur-able icephobic surfaces. Sci Adv. 2016;2:e1501496.

[6] Mazzola L. Aeronautical livery coating with icephobic property. Surf Eng. 2016;32(10):733–744. 2016.

[7] Bowden F, Hughes T. The mechanism of sliding on ice and snow. Proc R Soc London Ser A. 1939;172:280– 298.

[8] Colbeck SC. A review of the friction of snow skis. J Sports Sci. 1994;3(12):285–295.

[9] Kuzmin L. Interfacial kinetic ski friction [doctoral the-sis]. Mid Sweden University; 2010.

[10] De Koning G, De Groot GJ, Schenau JVI. Ice friction during speed skating. J Biomech. 1992;25(6):565–571.

[11] Slotfeldt-Ellingsen D, Torgersen L. Glide abilities of polyethylene ski base. Oslo: SINTEF; 1982. 62.

[12] Faraday M. On regelation, and on the conservation of force. Philosophical Magazine. Fourth Ser. 1859;17(I 13):162–69.

[13] Fierz C, Armstrong R L, Durand Y, et al. The inter-national classification for seasonal snow on the ground. IHP-VII Tech Doc Hydrol. 2009;83(1):1–80.

[14] Kietzig AM, Hatzikiriakos SG, Englezos P. Physics of ice friction. J Appl Phys. 2010;107:081101.

[15] Buhl D, Fauve MRH. The kinetic friction of polyethy-lene on snow: the influence of the snow temperature and the load. Cold Reg Sci Technol. 2001;33(2– 3):133–140.

[16] Bowden FP. Friction on snow and ice. Proc R Soc Lond A. 1953;217:462–478.

[17] Bäurle L, Szabò D, Fauve M, et al. Sliding friction of polyethilene on ice: tribometer measurements. Tribol Lett. 2006;24:77–84.

[18] Rohm SHM, Knoflach C, Van Putten J, et al. Friction between steel and snow in dependence of the steel roughness. Tribol Lett. 2015;59:27.

[19] Liang H, Martin JM, Mogne TL. Experimental investi-gation of friction in low-temperature ice. Acta Mater. 2003;51(9):2639–2646.

[20] Akkok M, Ettles CMM, Calabrese SJ. Parameters affecting the kinetic friction on ice. J Tribol. 1987;109 (3):552–561.

[21] Bäurle L, Kaempfer U, Szabó D, et al. Sliding friction of polyethylene on snow and ice: Contact area and mod-elling. Cold Reg Sci Technol. 2007;47:276–289.

[22] Evans DCB, Nye JF, Cheeseman KJ. The kinetic fric-tion of ice. Proc R Soc Lond. 1976;A 347:493–512.

[23] Makkonen M, Tikanmaki MM. Modeling the friction of ice. Cold Reg Sci Technol. 2014;102:84–93.

[24] Itagaki K, Lemieux GE, Huber NP. Preliminary study of friction between ice and sled runners. J Phys Colloques. 1987;48:297–301.

[25] Roberts AD, Richardson JC. Interface study of rubber-ice friction. Wear. 1981;67(1):55–69.

[26] Kuroiwa D. The kinetic friction on snow and ice. J Glaciol. 1977;19:141–152.

[27] Calabrese SJ, Buxton R, Marsh G. Frictional character-istics of materials sliding against ice. Lubr Eng. 1980;36
(5):283–289.
[28] Albracht F, Reichel S, Winkler V, et al. On the influ-ences of friction on ice. Materwiss und Werksttech. 2004;35(10–11):620–625.
[29] Montagnat M, Schulson EM. On friction and surface cracking during sliding of ice on ice. J Glaciol. 2003;49(166):391–396.
[30] Oksanen P, Keinonen J. The mechanism of friction of ice. Wear. 1982;78(3):315–324.
[31] Jones SJ, Kitagawa H, Izumiyama K, et al. Friction of melting ice. Ann Glaciol. 1994;19:7–12.
[32] Marmo BA, Farrow IS, Buckingham MP, et al. Frictional heat. Proc Inst Mech Eng Part L. 2006;220 (4):189–197.
[33] Ducret S, Zahouani H, Midol A, et al. Friction and abrasive wear of UHMWPE sliding on ice. Wear. 2005;258:26–31.
[34] Kietzig AM, Hatzikiriakos SG, Englezos P. Ice friction: the effects of surface roughness, structure and hydro-phobicity. J Appl Phys. 2009;106:024303.
[35] Kietzig AM, Hatzikiriakos SG, Englezos P. Patterned superhydrophobic metallic surfaces. Langmuir. 2009;25(8):4821–4827.
[36] Luo Y, Zhang D, Xu X, et al. Precise cutting micro-structured superhydrophobic surface. Surf Eng. 2016;32(2):119–124.
[37] Cohen N, Dotan A, Dodiuk H, et al. Superhydrophobic coatings and their durability. Mater Manuf Process. 2016;31(9):1143–1155.
[38] Khagendra T, Joshi B, Amanov A, et al. A Study on the effect of laser surface texturing on friction and wear behavior of graphite cast iron. J Tribol. 2016;I (138):011601.
[39] Shum PW, Zhou ZF, Li KY. To increase the hydropho-bicity and wear resistance of diamond-like carbon coatings by surface texturing using laser ablation pro-cess. Thin solid films. 2013;544:472–476.
[40] Braun D, Greinern C, Schneider J, et al. Efficiency of laser surface texturing in the reduction of friction under mixed lubrication. Tribol Int. 2014;77:142–147.
[41] Wang X, Kato K, Koshi A, et al. The effect of laser tex-turing of SiC surface on the critical load for the tran-sition of water lubrication mode from hydrodynamic to mixed. Tribol Int. 2001;34:703–711.
[42] Vandoni L, Demir AG, Previtali B, et al. Wear behavior of fiber laser textured TiN coatings in a heavy loaded sliding regime. Materials. 2012;5(11):2360–2382.
[43] Pawlak Z, Urbaniak W, Oloyede A. The relationship between friction and wettability in aqueous environ-ment. Wear. 2011;271:1745–1749.
[44] Chen YF, Chen YP, Zhang CB, et al. Influence of rough surface topography on wettability. J Eng Thermophys-Rus. 2011;32(7):1188–1190.
[45] Groten J, Rühe J. Surfaces with combined microscale and nanoscale structures: a route to mechanically stable superhydrophobic surfaces? Langmuir. 2013;29 (11):3765–3772.
[46] Öner D, McCarthy TJ. Ultrahydrophobic surfaces. Effects of topography length scales on wettability. Langmuir. 2000;16(20):7777–7782.
[47] Jopp J, Grüll H, Yerushalmi-Rozen R. Wetting behav-ior of water droplets on hydrophobic microtextures of comparable size. Langmuir. 2004;20:10015–10019.
[48] Luo BH, Shum PW, Zhou ZF, et al. Surface geometrical model modification and contact angle prediction for the laser patterned steel surface. Surf Coat Tech. 2010;205:2597–2604.
[49] Lawrence J, Li L. Wettability characteristics of poly-ethylene modified with CO_2, Nd:YAG, excimer and high-power diode lasers. Proc Instn Mech Engrs. 2015;215(Part B):1735–1744.
[50] Semaltianos NG, Perrie W, French P, et al. Femtosecond laser surface texturing of a nickel-based superalloy. Appl Surf Sci. 2008;255:2796–2802.
[51] Ta DV, Dunn A, Wasley TJ, et al. Nanosecond laser textured superhydrophobic metallic surfaces and their chemical sensing applications. Appl Surf Sci. 2015;357:248–254.
[52] Wang B, Wang X, Zheng H, et al. Surface wettability modification of cyclic olefin polymer by directfemtosecond laser irradiation. Nanomaterials. 2015;5:1442–1453.
[53] Wang YQ, Yang HF, Hao JB, et al. Experimental research on the fabrication and wettability of micro- and nano-scale surface textures produced on stainless steel using an ultrafast laser. Laser Eng. 2011;21:241– 254.

[54] Yang MZHF, Dai BJLJ, Cai ELZL. Forming mechan-isms and wettability of double-scale structures fabri-cated by femtosecond laser. Appl Phys A. 2009;94 (3):571–576.
[55] Demir AG, Furlan V, Lecis N, et al. Laser surface struc-turing of AZ31 Mg alloy for controlled wettability. Biointerphases. 2014;9(2):0290091.
[56] Furlan V, Demir AG, Previtali B. Micro and sub-micron surface structuring of AZ31 by laser re-melting and dimpling. Opt Laser Technol. 2015;75:164–172.
[57] Demir AG, Taketa TB, Tolouei R, et al. Laser surface structuring affects polymer deposition, coating hom-ogeneity, and degradation rate of Mg alloys. Materials Letters. 2015;160:359–362.
[58] Demir AG, Previtali B, Lecis N. Development of laser dimpling strategies on TiN coatings for tribological applications with a highly energetic Q-switched fibre laser. Opt Laser Technol. 2013;54:53–61.
[59] Yuan Y, Lee TR. Contact angle and wetting properties. In: G Bracco, B Holst, editors. Surface science tech-niques. Berlin: Springer; 2013. p. I–34.
[60] de Lara LR, Jagdheesh R, Ocaña JL. Corrosion resist-ance of laser patterned ultrahydrophobic aluminium surface. Mater Lett. 2016;184:100–103.
[61] Jagdheesh R, García-Ballesteros JJ, Ocaña JL. One-step fabrication of near superhydrophobic aluminum sur-face by nanosecond laser ablation. Appl Surf Sci. 2016;374:2–11.
[62] Kuzmin L. Interfacial kinetic ski friction [thesis for the degree of doctoral of philosophy]. Mid Sweden University; 2010.
[63] Mannion PT, Magee J, Coyne E, et al. The effect of damage accumulation behaviour on ablation thresholds and damage morphology in ultrafast laser micro-machining of common metals in air. Appl Surf Sci. 2004;233:275–287.
[64] Maressa P, Anodio L, Bernasconi A, et al. Effect of surface texture on the adhesion performance of laser treated Ti6Al4 V alloy. J Adhesion. 2015;91
(7):518–537.

Table 1. Mechanical properties of tested materials.

	AISI 301	Titanal
Sheet thickness (mm)	0.5	0.4
Brinell hardness HR	587.8	172
Tensile resistance (N mm^{-2})	1802	630
Yield strength (N mm^{-2})	1613	580

Table 2. Nominal chemical composition of AISI 301.

Element	C	Si	Mn	P	S	Cr	Ni	Others
wt-%	0.15	1.00	2.00	0.045	0.030	16.0/18.0	6.0/8.0	Bal.

Table 3. Nominal chemical composition of commercial Al alloy Titanal®.

Element	Al	Cu	Zn	Zr	Mg	Others
wt-%	88.6	1.7	7.00	0.1	2.5	Bal.

Table 4. Pulsed laser source features.

Wavelength	λ	1064 nm
Max. average power	P_{avg}	50 W
Pulse duration	τ	250 ns
Pulse repetition rate	PRR	20–80 kHz
Beam quality	M^2	1.7
Collimated beam diameter	d_C	5.9 mm
Focal length	f	100 mm
Focused beam diameter	d_0	39 µm

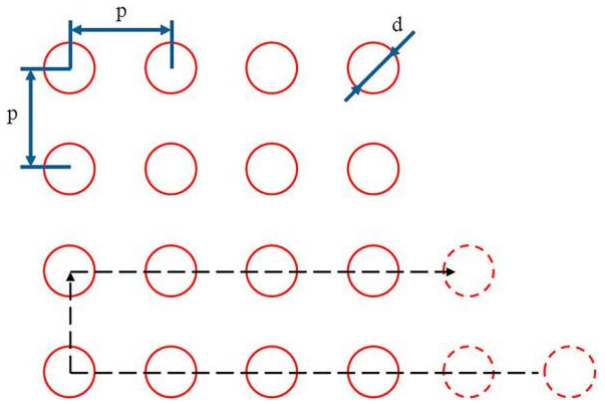

Figure 1. Schematic description of the laser produced surface patterning.

Table 5. Laser parameters used in percussion-drilling treatment.

Pump current	PI%	100%
Pulse repetition rate	PRR (kHz)	50
Dimple pitch	p (µm)	100
Jump delay	t_{delay} (µs)	8000
Focal height position	h_f (mm)	0
Modulation time	t_{mod} (µs)	30–80

Figure 2. An example of prototype miniature ski.

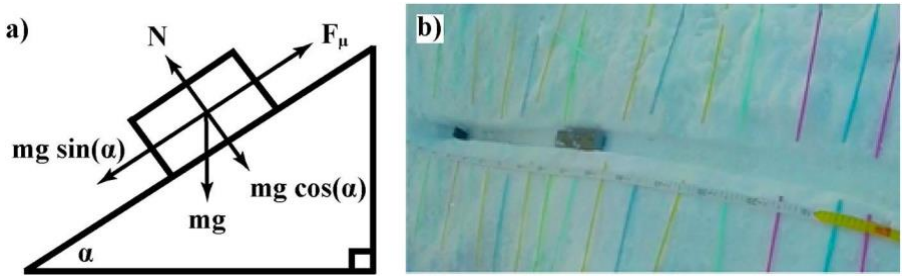

Figure 3. The simple dynamic model utilised to estimate the friction coefficient (a) and the snow track prepared for the tests (b)

Table 6. Environmental conditions for the field tests.

	Snow temperature (°C)	Relative humidity (−)
Test 1	2	82%
Test 2	−1	73%

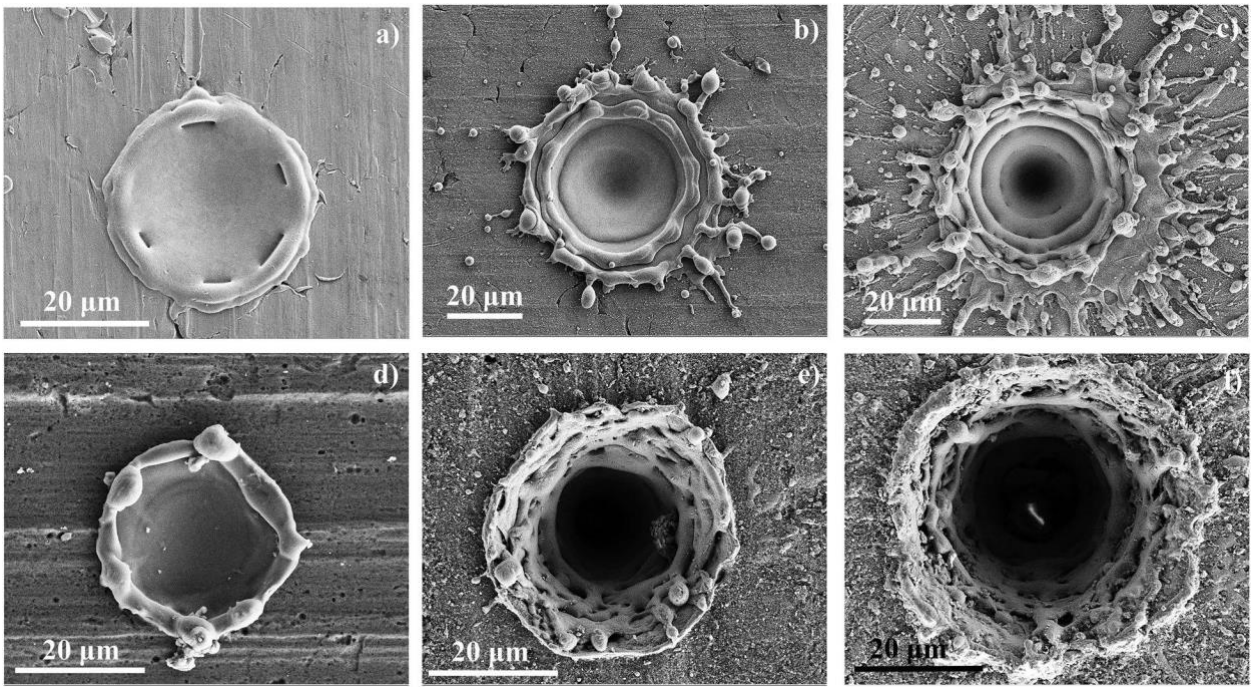

Figure 4. SEM images of some of the dimples realised. (a), (b) and (c) refer to samples in AISI 301. (d), (e) and (f) refer to samples in Titanal. Dimples (a) and (d) are obtained with t_{mod} = 45 µs. Dimples (b) and (e) are obtained with t_{mod} = 60 µs. Dimples (a) and (d) are obtained with t_{mod} = 80 µs.

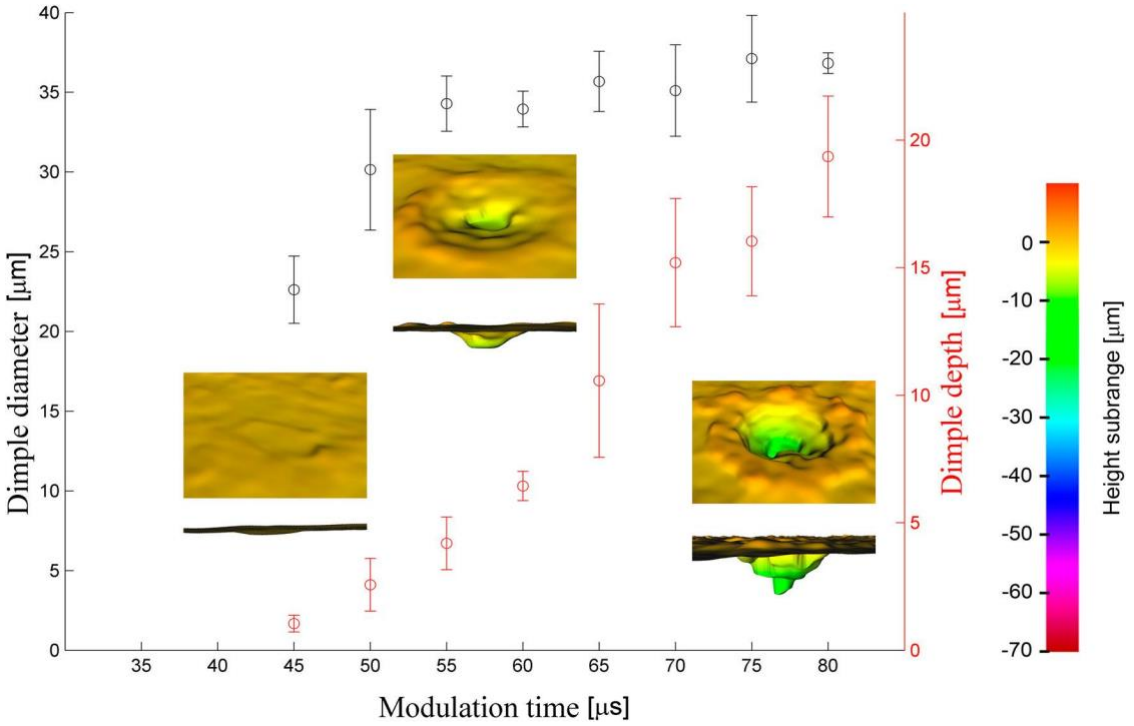

Figure 5. Sizes of dimples made on AISI 301 as a function of modulation time.

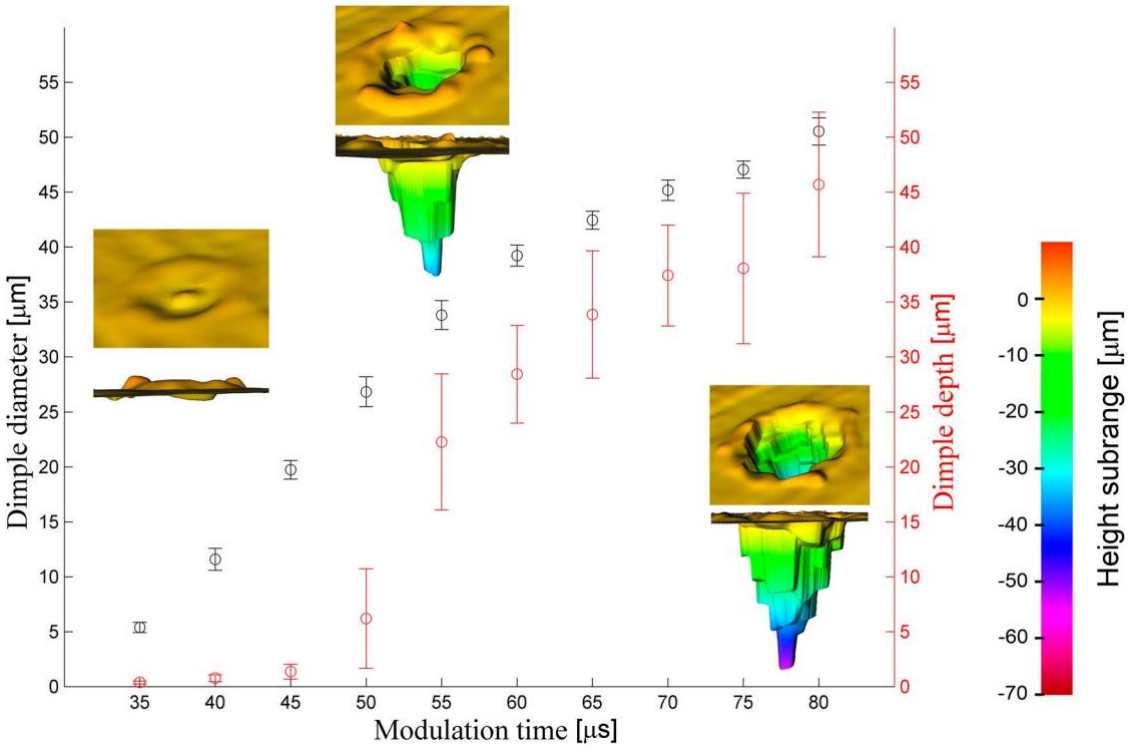

Figure 6. Sizes of dimple made on Titanal as a function of modulation time.

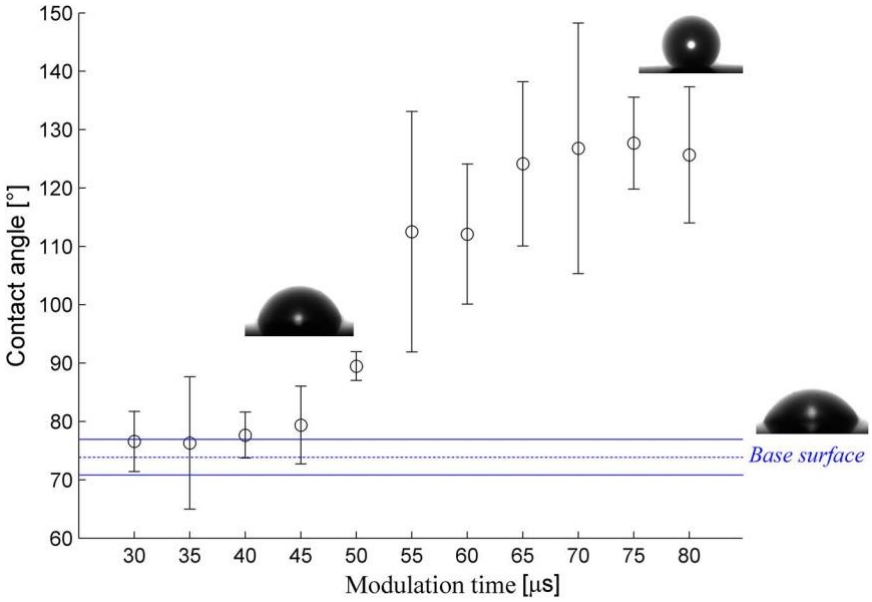

Figure 7. Contact angle of the textured AISI 301 samples obtained with different LST conditions.

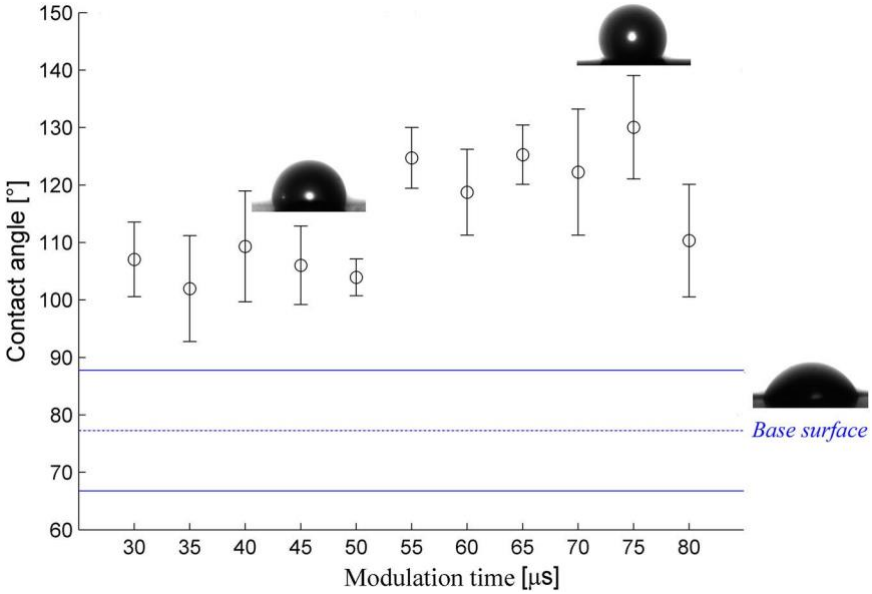

Figure 8. Contact angle of the textured Titanal samples obtained with different LST conditions.

Table 7. Contact angle for selected conditions before and after the burr removal process

	AISI 301		Titanal®	
t_{mod} (µs)	Before grinding	After sanding	Before grinding	After sanding
50	96 ± 8	93 ± 12	102 ± 5	101 ± 3
70	113 ± 20	112 ± 5	125 ± 12	124 ± 8

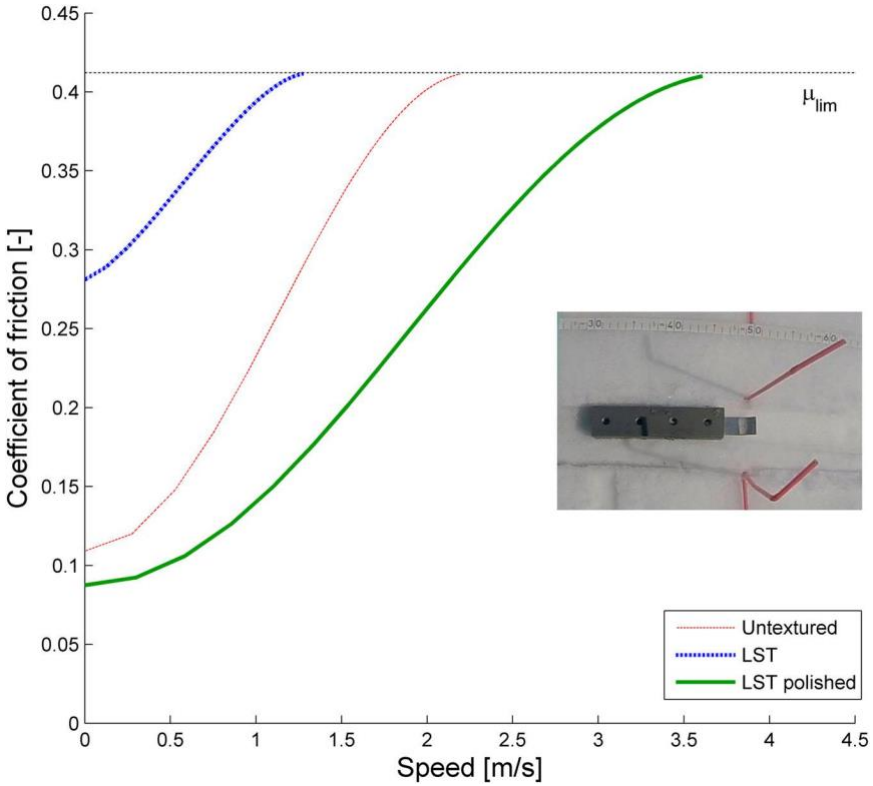

Figure 9. Friction coefficient versus speed for AISI 301 samples (Ambient conditions: air temperature: +10°C, snow temperature:

+2°C, relative humidity: 82%)

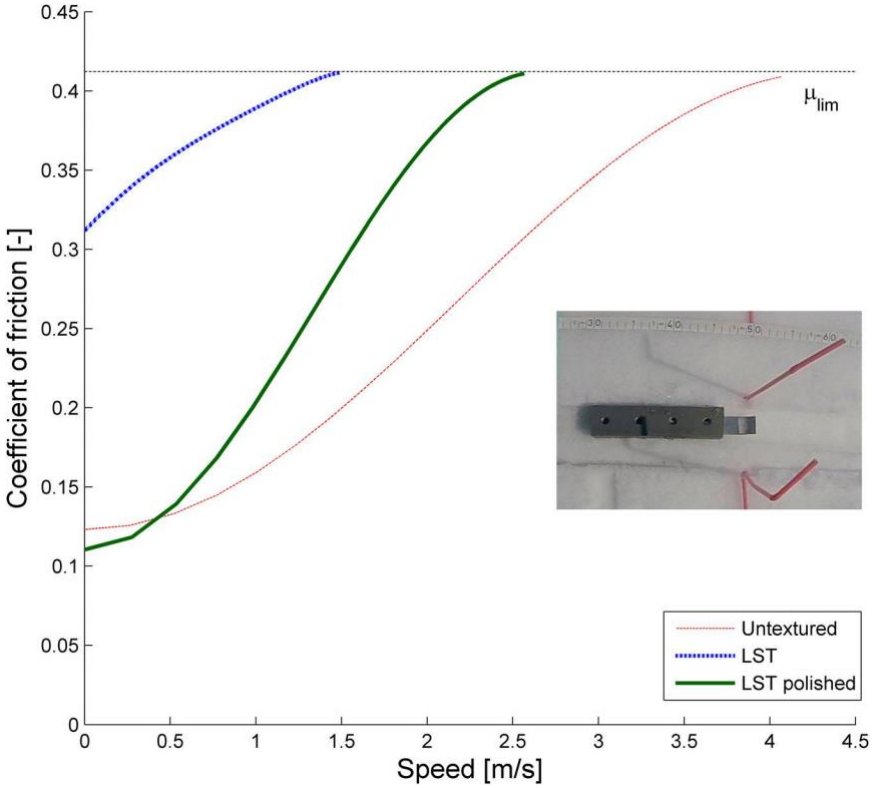

Figure 10. Friction coefficient versus speed for Titanal samples (Ambient conditions: air temperature: +10°C, snow temperature:

+2°C, relative humidity: 82%)

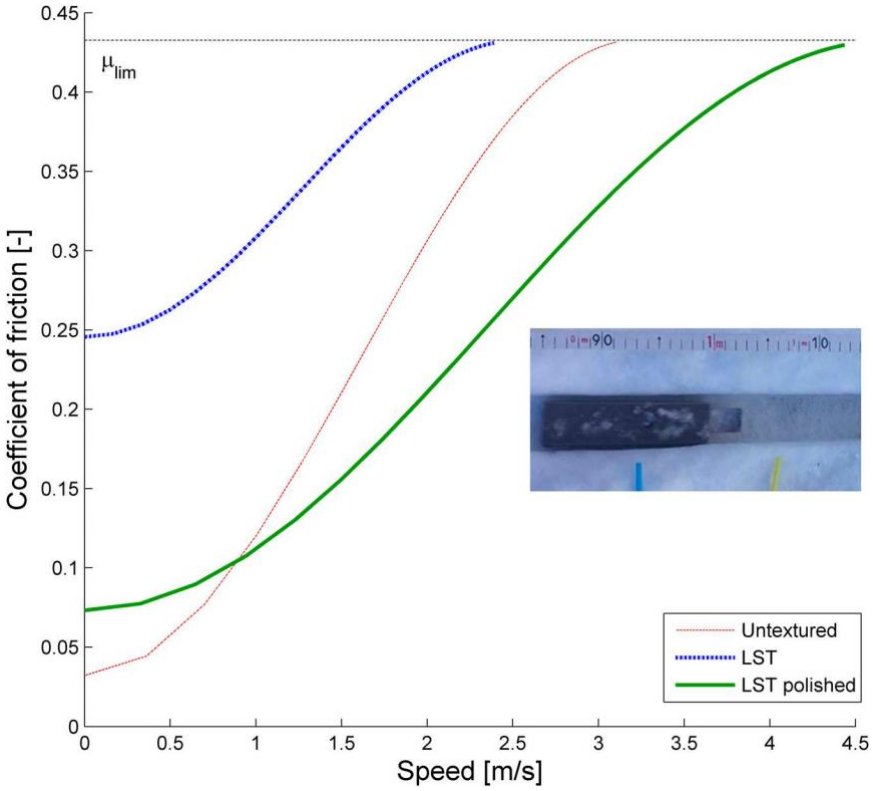

Figure 11. Friction coefficient versus speed for AISI 301 samples. (Ambient conditions: air temperature: −1°C, snow temperature: −1°C, relative humidity: 73%)

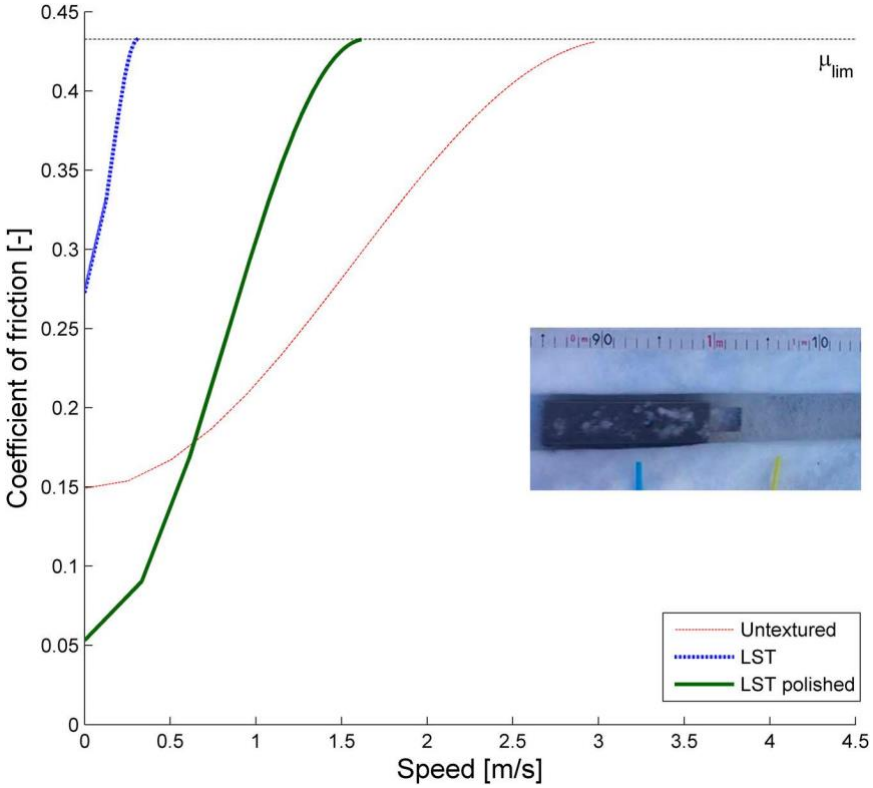

Figure 12. Friction coefficient versus speed for Titanal samples. (Ambient conditions: air temperature: −1°C, snow temperature: −1°C, relative humidity: 73%)